The viscous-convective subrange in nonstationary turbulence

J. R. Chasnov[a)]
The Hong Kong University of Science and Technology, Clear Water Bay, Kowloon, Hong Kong

(Received 10 November 1997; accepted 21 January 1998)

The similarity form of the scalar-variance spectrum at high Schmidt numbers is investigated for nonstationary turbulence. Theoretical arguments show that Batchelor scaling may apply only at high Reynolds numbers. At low Reynolds numbers, Batchlor scaling is not possible unless the turbulence is stationary or the enstrophy decays asymptotically as t^{-2}. When this latter condition is satisfied, it is shown from an analysis using both the Batchelor and Kraichnan models for the scalar-variance transfer spectrum that the k^{-1} power law in the viscous-convective subrange is modified. Results of direct numerical simulations of high Schmidt number passive scalar transport in stationary and decaying two-dimensional turbulence are compared to the theoretical analysis. For stationary turbulence, Batchelor scaling is shown to collapse the spectra at different Schmidt numbers and a k^{-1} viscous-convective subrange is observed. The Kraichnan model is shown to accurately predict the simulation spectrum. For nonstationary turbulence decaying at constant Reynolds number for which the enstrophy decays as t^{-2}, scalar fields for different Schmidt numbers are simulated in situations with and without a uniform mean scalar gradient. The Kraichnan model is again shown to predict the spectra in these cases with different anomalous exponents in the viscous-convective subrange. © *1998 American Institute of Physics.* [S1070-6631(98)01205-7]

I. INTRODUCTION

If the kinematic viscosity ν of a fluid is much greater than the diffusivity D of a scalar contaminant so that the Schmidt (or Prandtl) number $\sigma=\nu/D$ is large, then fluctuations in the scalar field will persist to much smaller length scales than those of the velocity. Almost forty years ago, Batchelor[1] considered the physics of a high Schmidt number fluid, and derived the now well-known k^{-1} viscous-convective subrange spectrum for wave numbers over which the velocity fluctuations are strongly damped by viscosity but diffusivity has not yet effectively smoothed the scalar fluctuations. Subsequent notable theoretical investigations of this subrange can be found in the papers of Saffman[2] and Kraichnan.[3,4]

Batchelor[1] argued that the effect of the large-scale velocity fluctuations on the small-scale scalar field could be represented as a persistent uniform strain. By further assuming that the scalar-variance spectrum was kept steady by the continual resupply of scalar-variance from lower wave numbers, he derived the form of the spectrum for wave numbers lying within the viscous subrange of the velocity field. Kraichnan[3] extended this investigation by considering the effects of fluctuations in the rates of strain in space and time. He showed that Batchelor's spectral form in the viscous-diffusive subrange, for which the smoothing effects of diffusivity are important, is substantially modified but the k^{-1} spectral form in the viscous-convective subrange remains unchanged. The insensitivity of the k^{-1} spectral law to the underlying representation of the velocity field suggests that this theoretical result may be exact.[4]

Early experiments using grid turbulence,[5] ocean measurements[6] and pipe turbulence[7] yielded reasonable agreement with the k^{-1} viscous-convective subrange spectrum. A more recent experiment measuring thickness fluctuations of a soap film in two-dimensional turbulence also yielded a k^{-1} spectral slope.[8] However, other recent experiments in a turbulent jet[9] and in mixing in two-dimensional turbulence,[10] both at very high Schmidt numbers, show no indication of a k^{-1} subrange. Numerical experiments in forced statistically stationary turbulence[11–13] support the existence of a k^{-1} subrange, although decaying flow simulations do not.[14] Part of the purpose of this present paper is to establish conditions for which nonstationary turbulence may exhibit Batchelor's k^{-1} viscous-convective subrange spectrum.

Batchelor's[1] seminal work on the large Schmidt number passive scalar and also subsequent theoretical work[2–4] explicitly assumed a steady scalar-variance spectrum in the viscous subrange. In light of the contradictory experimental evidence, an important question arises as to just how stationary the flow statistics must be for an assumption of steadiness to be reasonable. For instance, the concept of a universal statistical equilibrium of the small scales of a high Reynolds number three-dimensional turbulence is well-known.[15] The characteristic time of inertial range eddies at high Reynolds numbers can be written as $(k^3E(k,t))^{-1/2}$, where $E(k,t)$ is the usual three-dimensional energy spectrum, and in the inertial subrange $E\propto k^{-5/3}$ so that the characteristic time decreases as $k^{-2/3}$. At high Reynolds number, the inertial range is of lengthy extent so that one can expect that the short time scale of the inertial range eddies relative to that of the overall energy decay makes an equilibrium assumption reasonable.

The above argument can be made more quantitative, and

[a)]Phone: (852) 23587448; Fax: (852) 23581643; electronic mail: chasnov@math.ust.hk

it is useful to do so here for later comparison with the scalar result. For wave numbers lying within the equilibrium subrange, external sources of energy production may be neglected and the energy spectrum evolution equation can be written as

$$\frac{\partial}{\partial t}E(k,t)=T(k,t)-2\nu k^2E(k,t), \tag{1}$$

where $T(k,t)$ represents the nonlinear transfer spectrum. The Kolmogorov similarity hypothesis for three-dimensional turbulence supposes that the energy and transfer spectrum scales with the energy dissipation rate ϵ and the viscosity ν, alone. One has dimensionally

$$E(k,t)=(\epsilon\nu^5)^{1/4}\hat{E}(\hat{k}), \quad T(k,t)=(\epsilon\nu)^{3/4}\hat{T}(\hat{k}), \tag{2}$$

with

$$\hat{k}=k/k_d, \quad k_d=(\epsilon/\nu^3)^{1/4}, \tag{3}$$

where k_d is the Kolmogorov, or dissipation, wave number. Viscous forces strongly damp the Fourier components of the velocity fluctuations for $k\gg k_d$. The similarity spectra $\hat{E}(\hat{k})$ and $\hat{T}(\hat{k})$ are assumed to be stationary in the rescaled coordinates.

Changing independent variables in (1) from (k,t) to $(\hat{k},t')$, with $t'=t$, using

$$\frac{\partial}{\partial t}=\frac{\partial}{\partial t'}-\frac{1}{4}\epsilon^{-1}\frac{d\epsilon}{dt'}\,\hat{k}\,\frac{\partial}{\partial\hat{k}}, \tag{4}$$

Eq. (1) is transformed into

$$x\left[\hat{k}\,\frac{d}{d\hat{k}}\,\hat{E}(\hat{k})-\hat{E}(\hat{k})\right]=\hat{T}(\hat{k})-2\hat{k}^2\hat{E}(\hat{k}), \tag{5}$$

with

$$x=\frac{1}{2}\,\frac{d}{dt}(\nu/\epsilon)^{1/2}. \tag{6}$$

If $x=x(t)$ depends explicitly on time as would commonly be expected for a nonstationary turbulence, then (5) contradicts the assumption that the similarity spectra are stationary. However, if one supposes that the dissipation rate ϵ is independent of viscosity in the limit $\nu\to 0$ as is usually assumed for three-dimensional turbulence, then x goes to zero as $\nu^{1/2}$ so that the time-dependent left-hand side of (5) becomes negligible with respect to the right-hand side at sufficiently high Reynolds numbers. A stationary similarity state can then exist, and a quasi-steady assumption for the spectrum $(x=0)$ is appropriate.

However, the physics of the viscous-convective subrange for large Schmidt numbers differs notably from the inertial subrange. The characteristic time scale of a scalar blob in this subrange is independent of wave number, being set by the time scale associated with the large-scale straining of the velocity field. A statistical equilibrium for the scalar field may not occur even if the diffusivity D goes to zero if the Reynolds number of the turbulence is not sufficiently large. This point will be made quantitative in the following section, where we derive an explicit criterion which must be satisfied before the scalar-variance spectrum can be assumed quasi-steady.

II. STATISTICAL EQUILIBRIUM OF THE SCALAR

The passive scalar transport equation is given by

$$\frac{\partial\theta}{\partial t}+\boldsymbol{\nabla}\cdot(\mathbf{u}\theta)=D\nabla^2\theta+f_\theta, \tag{7}$$

where $\mathbf{u}$ is the turbulent velocity field and f_θ represents some generic source of scalar fluctuations. The time-evolution equation for the spherically-integrated scalar-variance spectrum $E_\theta(k,t)$ obtained from (7) may be written as

$$\frac{\partial}{\partial t}E_\theta(k,t)=T_\theta(k,t)-2Dk^2E_\theta(k,t)+F_\theta(k,t), \tag{8}$$

where $T_\theta(k,t)$ is the scalar-variance transfer spectrum, $F_\theta(k,t)$ is the production spectrum of scalar variance, and E_θ has been defined so that the scalar variance is twice its integral:

$$\langle\theta^2\rangle=\int_0^\infty 2E_\theta(k,t)\,dk. \tag{9}$$

We also define here the scalar-variance dissipation and production rates, ϵ_θ and ϵ_θ^f, respectively, by

$$\epsilon_\theta=2D\int_0^\infty k^2E_\theta(k,t)\,dk, \quad \epsilon_\theta^f=\int_0^\infty F_\theta(k,t)\,dk; \tag{10}$$

so that $\frac{1}{2}d\langle\theta^2\rangle/dt=\epsilon_\theta^f-\epsilon_\theta$. The dissipation and production rates are unequal if the scalar statistics are nonstationary. For the remainder of this work, we assume that the production spectrum $F_\theta(k,t)$ is negligible in the viscous subrange.

Following Batchelor,[1] we suppose that for large Schmidt numbers the scalar-variance and transfer spectra in the viscous subrange of the velocity field can be made stationary in coordinates scaled by the scalar-variance dissipation rate ϵ_θ, the diffusivity D, and a rate-of-strain parameter that we take here to be $(\epsilon/\nu)^{1/2}$, which completely characterizes the effect of the large-scale velocity field on the small-scale scalar field.

Now from dimensional analysis, one obtains

$$\begin{aligned}E_\theta(k,t)&=\epsilon_\theta D^{1/2}(\nu/\epsilon)^{3/4}\hat{E}_\theta(\hat{k}),\\ T_\theta(k,t)&=\epsilon_\theta D^{1/2}(\nu/\epsilon)^{1/4}\hat{T}_\theta(\hat{k}),\end{aligned} \tag{11}$$

with

$$\hat{k}=k/k_B; \quad k_B=(\epsilon/\nu D^2)^{1/4}, \tag{12}$$

where k_B is called the Batchelor wave number. Diffusion strongly damps the scalar fluctations for $k\gg k_B$. Again, the similarity spectra $\hat{E}_\theta(\hat{k})$ and $\hat{T}_\theta(\hat{k})$ are assumed to be stationary. Although we use the same symbol $\hat{k}$ for the scaled wave number as previously, the two definitions differ by a factor of $\sigma^{1/2}$.

Changing variables in (8) from (k,t) to $(\hat{k},t')$ using (4), Eq. (8) (with F_θ negligible) is transformed into

$$(y+3x)\hat{E}_\theta(\hat{k})+x\hat{k}\,\frac{d}{d\hat{k}}\,\hat{E}_\theta(\hat{k})=\hat{T}_\theta(\hat{k})-2\hat{k}^2\hat{E}_\theta(\hat{k}), \quad (13)$$

with x defined in (6) and

$$y=(\nu/\epsilon)^{1/2}\epsilon_\theta^{-1}\frac{d\epsilon_\theta}{dt}. \quad (14)$$

For a general nonstationary flow, $x=x(t)$ and $y=y(t)$ are explicit functions of time and (13) contradicts the assumption of stationary similarity spectra. We encountered this difficulty before when considering the energy spectrum in the universal equilibrium subrange (5). There we noted that an assumption of high Reynolds numbers ($\nu\to 0$) in three-dimensional turbulence was sufficient to permit the existence of a similarity state. Again we find that high Reynolds numbers are required for x and y to be negligibly small in nonstationary flow since in three dimensions they are both proportional to $\nu^{1/2}$. Both x and y are independent of the diffusivity D as $D\to 0$ so large Schmidt numbers by themselves are insufficient to admit a similarity state solution.

For conditions of a nonstationary turbulence at low-to-moderate Reynolds numbers, we must conclude that in general Batchelor's similarity state of the form (11) cannot occur even though the Schmidt number may be large. However, a special situation could arise if x and y in (6) and (14) are constant in time. This is possible only in one of two ways. First, the enstrophy, ϵ/ν, is constant in time so that $x=0$, and ϵ_θ decays exponentially so that y is a nonzero constant. Second, the enstrophy becomes asymptotically proportional to t^{-2} during the turbulence decay so that x is a nonzero constant, and ϵ_θ evolves as a power law in time so that y is constant (possibly zero). Interestingly, a t^{-2} decay law for the enstrophy was recently found[18] for decaying two-dimensional turbulence at constant Reynolds number. Thus this two-dimensional decaying flow provides a good way to test the above theoretical analysis, and it is of use to understand the theoretical consequences of nonzero constant values of x and y, which we do now in the next section.

III. APPLICATION OF THE BATCHELOR AND KRAICHNAN TRANSFERS TO NONSTATIONARY FLOW

A. The Batchelor transfer

Implicit in Batchelor's work on high Schmidt number fluids is a form for $T_\theta(k,t)$ in the viscous subrange:[1,2]

$$T_\theta^B=-\alpha(\epsilon/\nu)^{1/2}\frac{\partial}{\partial k}(kE_\theta), \quad (15)$$

where α^{-1} is the nondimensional proportionality constant appearing in the k^{-1} viscous-convective subrange spectrum. For three-dimensional turbulence, Batchelor originally estimated $\alpha^{-1}\approx 2$, while Gibson,[16] by considering the root mean square of the local values of the least principle rate of strain, proposed the bounds

$$\sqrt{3}<\alpha^{-1}<2\sqrt{3}. \quad (16)$$

Using the Batchelor form for the transfer spectrum and (11), Eq. (13) becomes

$$(\alpha+x)\hat{k}\,\frac{d}{d\hat{k}}\,\hat{E}_\theta(\hat{k})=-(\alpha+3x+y+2\hat{k}^2)\hat{E}_\theta(\hat{k}), \quad (17)$$

which may be integrated if x and y are constants. The solution is

$$\hat{E}_\theta(\hat{k})=c\hat{k}^{-(1+z)}\exp[-\hat{k}^2/(\alpha+x)], \quad (18)$$

where

$$z=(2x+y)/(\alpha+x). \quad (19)$$

A nonzero constant value of z results in a deviation from the Batchelor k^{-1} viscous-convective subrange spectrum. The constant c may be determined by imposing the normalization condition

$$\int_0^\infty \hat{k}^2\hat{E}_\theta(\hat{k})d\hat{k}=\frac{1}{2}; \quad (20)$$

one finds

$$c=[(\alpha+x)^{1-z/2}\Gamma(1-z/2)]^{-1}, \quad (21)$$

where Γ is the usual gamma function, and $\Gamma(1)=1$. For stationary flow, $x=y=z=0$, $c=\alpha^{-1}$, and (18) reduces to the original Batchelor spectrum[1] in the viscous subrange of a large Schmidt number fluid.

The form of the spectrum in the viscous-convective subrange for which the effects of molecular diffusivity are negligible may be recovered from (18) in the limit of small $\hat{k}$, for which the exponential factor approaches unity. The dimensional form is

$$E_\theta(k,t)=c\,\epsilon_\theta(\nu/\epsilon)^{1/2}k^{-1}(k/k_B)^{-z}, \quad (22)$$

where k_B is given by (12). Equation (22) differs from the Batchelor k^{-1} spectral form by a factor of $(k/k_B)^{-z}$.

The viscous-convective subrange form (22) presents a paradox in that this subrange should be independent of the diffusivity D, whereas k_B depends on D. A resolution of this paradox is obtained by assuming that the scalar-variance dissipation rate ϵ_θ remains an explicit function of D even as $D\to 0$. That is, for D to cancel from (22), ϵ_θ must scale like

$$\epsilon_\theta=\sigma^{-z/2}\chi, \quad (23)$$

as $\sigma\to\infty$, where χ is independent of σ in this limit. This explicit scaling of ϵ_θ on σ is simply a dimensional consequence of Batchelor scaling and a spectral power law different than k^{-1}.

B. The Kraichnan transfer

Considering the effect of fluctuations in the rate of strain in space and time, Kraichnan[3,4] proposed a model for the transfer spectrum in the viscous-convective subrange which differs from the Batchelor form, (15), yet still satisfies Batchelor scaling, (11). Kraichnan's transfer spectrum for turbulence in N spatial dimensions can be written as[4]

$$T_\theta^K=-\alpha(\epsilon/\nu)^{1/2}\frac{\partial}{\partial k}\left[kE_\theta-\frac{k}{N}\frac{\partial}{\partial k}(kE_\theta)\right]. \quad (24)$$

As observed directly from (24), the Batchelor form for the transfer (15) is recovered as the number of spatial dimensions N approaches infinity. Here, we will consider the physically interesting values $N=2$ and 3, corresponding to two- and three-dimensional turbulence. The Kraichnan transfer vanishes both in the k^{-1} viscous-convective subrange and when $E_\theta(k)\propto k^{N-1}$, corresponding to an equipartition distribution of scalar-variance. Batchelor's transfer only vanishes for the k^{-1} spectrum. The k^{N-1} spectrum appears in numerical simulations of the scalar equation when the diffusivity is taken to be identically zero and all the Fourier components of the scalar field with wave number magnitude greater than some given k_m are truncated. The Kraichnan transfer has the potential to predict the scalar-variance spectrum resulting from this (unphysical) numerical experiment while the Batchelor transfer does not. In this sense, one can view the Kraichnan model as providing additional physics which is missing from the original Batchelor model.

Analytical solution of the equations using the Kraichnan form for the transfer spectrum is somewhat more complicated than that for the Batchelor form and it is worthwhile first to review the results for stationary flow.[4,17] Using (11), (13), and (24) with $x=y=0$, one has

$$\alpha\frac{d}{d\hat{k}}\left[\hat{k}\hat{E}_\theta(\hat{k})-\frac{\hat{k}}{N}\frac{d}{d\hat{k}}(\hat{k}\hat{E}_\theta(\hat{k}))\right]+2\hat{k}^2\hat{E}_\theta(\hat{k})=0. \quad (25)$$

Simplification of (25) is possible by changing variables to

$$r=(2N\alpha^{-1})^{1/2}\hat{k}, \quad \hat{E}_\theta=\alpha^{-1}\hat{k}^{-1}f(r), \quad (26)$$

after which (25) is transformed to

$$f''-\frac{(N-1)}{r}f'-f=0, \quad (27)$$

where the prime denotes differentiation with respect to r. Boundary conditions are given by $f(\infty)=0$, and from the normalization condition (20), which becomes

$$\int_0^\infty rf(r)dr=N. \quad (28)$$

Multiplying (27) by r, integrating, and applying the boundary condition at infinity, the normalization condition (28) above is determined to be equivalent to $f(0)=1$.

For $N=3$, the unique solution to (27) which satisfies the above boundary conditions is given by

$$f(r)=(1+r)\exp(-r); \quad (29)$$

for $N=2$, a correspondingly simple analytical solution is unobtainable. However, asymptotic solutions for small and large r can be determined to be

$$f(r)=(1+\tfrac{1}{2}r^2\ln r+O(r^2)), \quad r\to 0; \quad (30)$$

$$f(r)\propto r^{1/2}\exp(-r), \quad r\to\infty. \quad (31)$$

Numerical solution for $f(r)$ over the full range of r is most easily obtained by integrating (27) from a sufficiently large value of r so that (31) is valid, to zero, and adjusting the unknown proportionality constant in (31) to make $f(0)=1$. We will make use of such a numerical solution for f in Sec. IV when we compare the Kraichnan spectrum to our forced two-dimensional numerical simulations.

For nonstationary flow with constant x and y, the change of variables given by (26) transforms (13) into

$$r^2f''-\left[N-1+\frac{Nx}{\alpha}\right]rf'-\left[r^2+\frac{N(2x+y)}{\alpha}\right]f=0, \quad (32)$$

with boundary condition $f(\infty)=0$ and normalization condition (28). The viscous-convective subrange behavior ($r\to 0$) of the spectrum is found from (32) by neglecting the r^2f diffusion term. Equation (32) then becomes an Euler equation with solution

$$f(r)\propto r^{-s}, \quad (33)$$

corresponding to a viscous-convective subrange of the form $k^{-(1+s)}$. Obtaining the quadratic equation for s, and choosing the root so that the Batchelor transfer solution $s=z$, with z given by (19), is obtained as $N\to\infty$, one determines

$$s=\frac{N(\alpha+x)}{2\alpha}\left[\left(1+\frac{4\alpha z}{N(\alpha+x)}\right)^{1/2}-1\right]. \quad (34)$$

Kraichnan's transfer spectrum thus predicts for nonzero x or y a modification to the viscous-convective subrange spectrum different than the Batchelor transfer spectrum (see (18) and (19)), though both yield a k^{-1} spectrum for stationary flow.

The asymptotic solution of (32) as $r\to\infty$ is given by

$$f(r)\propto r^{(1/2)(N-1+Nx/\alpha)}\exp(-r), \quad (35)$$

which reduces to the asymptotic forms obtained from (29) and (31) when $x=0$ and $N=3$ or 2, respectively.

A complete solution for $f(r)$ requires numerical integration of (32) from some large value of r using initial conditions obtained from (35), into zero, with known values of α, x and y. The proportionality constant in (35) is obtained by requiring $f(r)$ to satisfy the normalization condition given by (28). Such a numerical solution will be obtained in Secs. VI and VII, when we compare the above theoretical results to numerical simulation data.

The following sections test the theoretical ideas just developed. In Sec. IV, numerical simulations of forced two-dimensional turbulence with quasi-stationary velocity and scalar statistics are presented and compared to the Batchelor and Kraichnan theoretical results. The Kraichnan result is found to be superior, and a numerical value for α, the only free parameter in the model, is determined. In Secs. V–VII, the theoretical results are compared to numerical simulations of nonstationary, decaying two-dimensional turbulence at constant Reynolds number.

IV. PASSIVE SCALAR TRANSPORT BY QUASI-STATIONARY TWO-DIMENSIONAL TURBULENCE

We now present results from numerical simulations of passive scalar transport by forced two-dimensional turbulence at low Reynolds numbers to assess the accuracy of Batchelor scaling and to attempt and exhibit explicitly the spectral form k^{-1} in the viscous-convective subrange. These

present calculations confirm and supplement previous work by Holzer and Siggia[11] which found a k^{-1} subrange for a forced passive scalar field dissipated by hyperdiffusion and transported by a two-dimensional velocity field evolved by solving a restricted Euler equation.

The pseudo-spectral numerical method used here to simulate a two-dimensional turbulent velocity field in a periodic square of length 2π is described in Chasnov.[18] The Fourier transforms of the (forced) vorticity and scalar equations are integrated in time using

$$\frac{\partial}{\partial t}[\hat{\omega}\ \exp(\nu k^2 t)] = -\exp(\nu k^2 t)[\widehat{\nabla\cdot(\mathbf{u}\omega)} + \hat{f}_\omega], \tag{36}$$

$$\frac{\partial}{\partial t}[\hat{\theta}\ \exp(Dk^2 t)] = -\exp(Dk^2 t)[\widehat{\nabla\cdot(\mathbf{u}\theta)} + \hat{f}_\theta], \tag{37}$$

where $k=\sqrt{k_1^2+k_2^2}$ and the carets denote the Fourier coefficients at wave number $\mathbf{k}$. The Fourier transforms of the vorticity forcing term $\hat{f}_\omega(\mathbf{k},t)$ and scalar forcing term $\hat{f}_\theta(\mathbf{k},t)$ are taken to be delta-function correlated in time. Their numerical implementation are given by

$$\hat{f}_\omega(\mathbf{k}) = \left[\frac{F_\omega(k)}{\pi k(\delta t)}\right]^{1/2} \exp(i2\pi R_1), \tag{38}$$

$$\hat{f}_\theta(\mathbf{k}) = \left[\frac{F_\theta(k)}{\pi k(\delta t)}\right]^{1/2} \exp(i2\pi R_2), \tag{39}$$

where δt is the time-interval over which $\hat{f}_\omega$ and $\hat{f}_\theta$ are kept constant, and R_1 and R_2 are random uniform deviates chosen independently at the beginning of each time interval subject to the complex conjugate symmetry of $\hat{f}_\omega$ and $\hat{f}_\theta$. The forcing spectra $F_\omega(k)$ and $F_\theta(k)$ are specified to be

$$F_\omega(k) = \frac{\eta^f}{(2\pi)^{1/2}\sigma}\exp[-(k-k_f)^2/2\sigma^2], \tag{40}$$

$$F_\theta(k) = \frac{\epsilon_\theta^f}{(2\pi)^{1/2}\sigma}\exp[-(k-k_f)^2/2\sigma^2], \tag{41}$$

where η^f and ϵ_θ^f are the average production rates of one-half the mean-square vorticity and scalar variance, k_f is the forcing wave number, and σ is the width of the forcing in wave space. In the computations presented here, η^f ϵ_θ^f and σ are taken to be unity, and $k_f=4$.

The time integration is performed using the standard fourth-order four-step Runge–Kutta method, so that the random numbers generated in the second step are used without change in the third step (both steps occurring at the middle of the time interval), and the random numbers regenerated at the fourth step are used again in the first step of the next integration. The time interval δt is given by $\delta t=\Delta t/2$, where Δt is the time step associated with each integration step, determined at the beginning of each step using a Courant–Friedrichs–Lewy condition (see Ref. 18 for details). Multiple realizations of the vorticity and scalar fields are evolved simultaneously until the statistics become quasi-stationary, after which time averaging is performed. It was difficult to obtain truely stationary two-dimensional turbulence and the turbulent energy was observed to slowly drift upwards over long-time scales. Schmidt numbers simulated correspond to $\sigma=1$, 10, 100 and 1000. The largest Schmidt number simulation was performed using 1024^2 grid points and 16 independent realizations of the velocity and scalar fields. The Reynolds number of the turbulence, defined as

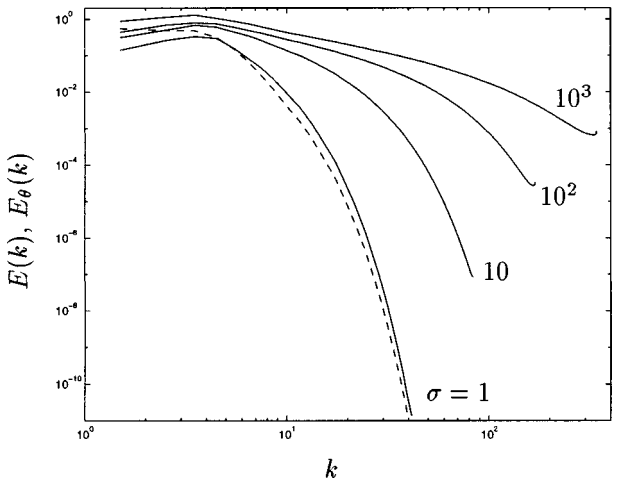

FIG. 1. Enstrophy and scalar-variance spectra for forced two-dimensional turbulence. The enstrophy spectrum is represented by the dashed line and the scalar-variance spectra by the solid lines, labeled by their respective Schmidt numbers.

$$R = \frac{\langle \mathbf{u}^2\rangle}{\langle\omega^2\rangle^{1/2}\nu}, \tag{42}$$

had values lying between $25<R<65$, corresponding to a relatively low Reynolds number turbulence. The range in R corresponds to a drift upwards in the Reynolds number over long time scales. The higher Schmidt number scalars were simulated by restarting the calculations using interpolated fields saved at lower Schmidt numbers (and lower resolutions), so that the net effect is that the lower Schmidt number runs were performed in the lower range of Reynolds numbers and the higher Schmidt number runs in the upper range. The lack of exact stationarity of the energy statistics does not seem to have had a major impact on our results, apparently because the viscous subrange of the scalar-variance spectrum is quasi-stationary due to the smallness of the nondimensional groups $x(t)$ and $y(t)$ as discussed in Sec. II.

In Fig. 1, a representative enstrophy spectrum (dashed line) and the scalar-variance spectra (solid lines) for the different Schmidt numbers are plotted. It is evident that as the Schmidt number increases, the scalar-variance containing scales extend to much larger wave numbers than the enstrophy containing scales. For $\sigma=1$, the enstrophy and scalar-variance spectra are comparable, though it is to be noted that the enstrophy spectrum is larger than the scalar-variance spectrum at the smallest wave numbers. This is presumably a consequence of the inverse energy cascade of two-dimensional turbulence without an analagous inverse cascade of scalar variance. The finite size of the periodic computational box prevents the inverse cascade of energy to ever larger-and-larger scales.[19] In an infinite box, the energy of the turbulence would increase indefinitely, and it is likely that the difficulty in attaining statistically-stationary energy

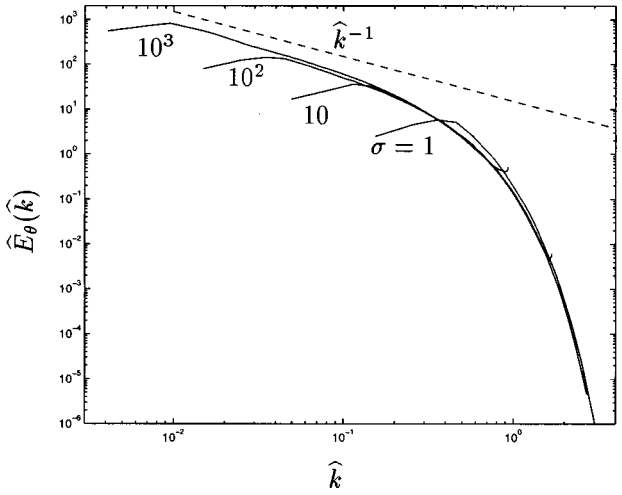

FIG. 2. Batchelor-scaled scalar-variance spectra for forced two-dimensional turbulence. A $\hat{k}^{-1}$ spectrum is seen to appear for $\hat{k} \ll 1$.

statistics is due to the inverse cascade. The scalar field at the highest Schmidt number $\sigma = 1000$ is somewhat underresolved.

In Fig. 2, the wave numbers and scalar-variance spectra are rescaled using Batchelor scaling, (11). Note that the rate-of-strain parameter $(\epsilon/\nu)^{1/2}$ is equal to the root-mean-square-vorticity $\langle \omega^2 \rangle^{1/2}$, which is a more meaningful representation in two-dimensional turbulence. Apart from wave numbers less than or close to the forced wave numbers, a reasonable collapse of the spectra for the different Schmidt numbers is observed. As $\hat{k} \to 0$, an approximate inertial-convective subrange proportional to $\hat{k}^{-1}$ is seen as expected for stationary turbulence.

In Fig. 3, we display a fit of the Kraichnan theoretical scalar-variance spectrum discussed in Sec. III to the $\sigma = 100$ numerical results obtained by minimizing the mean-squared error between the theoretical and simulation scalar-variance dissipation spectra $(\hat{k}^2 \hat{E}_\theta)$ as a function of the single free parameter α in the Kraichnan model. Only the data for wave numbers greater than eight were used (corresponding to the eighth point in Fig. 3). We have determined that the best fit to this particular simulation spectrum occurs for the value $\alpha^{-1} = 6.0$. In the figure, the resulting Kraichnan scalar-variance dissipation spectrum (solid line) is compared to the numerical simulation spectrum (points), and excellent agreement is observed. For comparison, the Batchelor spectrum (dashed line) with $\alpha^{-1} = 6.0$ is also plotted, and it is evident that the Kraichnan spectrum provides a much better fit to the data. Lowering the value of α can reduce the error between the Batchelor spectrum and simulation results, but the fit remains relatively poor.

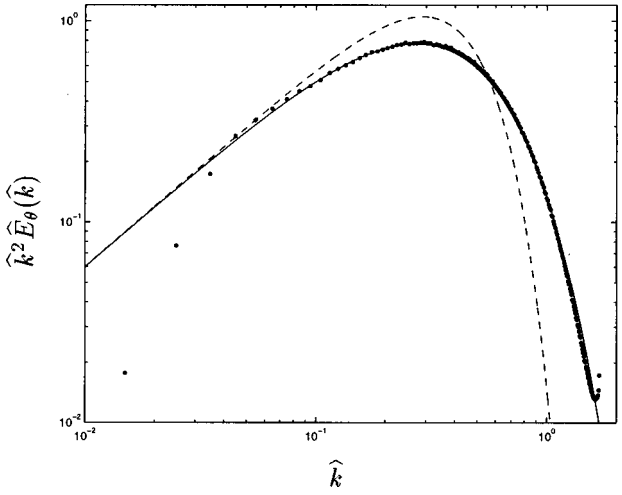

FIG. 3. Batchelor-scaled scalar-variance dissipation spectrum for forced two-dimensional turbulence with $\sigma = 100$. Numerical simulation results (points) are compared to the Kraichnan spectrum (solid line) and Batchelor spectrum (dashed line) with $\alpha^{-1} = 6.0$.

A comparison between numerical simulations and theoretical spectra was recently presented by Bogucki *et al.*[13] for three-dimensional turbulence with rather similar results. In that work, a least-squares fit of the Kraichnan spectrum to the simulation data resulted in a value of $\alpha^{-1} = 5.26$, which is not much different than the value of 6.0 obtained here. The Batchelor spectrum was also observed to give a relatively poorer fit. We also note that the best fit value of α^{-1} from our simulation data depends slightly on the Reynolds number of the flow field. This is presumably a low Reynolds number effect.

For simplicity, in the remainder of this paper we take as our theoretical model the Kraichnan form of the transfer spectrum, (24), with $\alpha^{-1} = 6.0$. In the following sections, we will compare the results of this model to the transport of high Schmidt number scalar fields in nonstationary flow situations.

V. DECAYING TWO-DIMENSIONAL TURBULENCE AT CONSTANT REYNOLDS NUMBER

We begin our numerical study of nonstationary flow by first reviewing the physics of two-dimensional turbulence decay at constant Reynolds number. Previously[18] we showed that for an initial two-dimensional flow field less than a transitional, or critical, Reynolds number R_c, linear final period of decay solutions result for which the Reynolds number $R(t)$, defined in (42), decreases to zero asymptotically. For initial Reynolds numbers greater than R_c, the flow field evolves with asymptotically increasing $R(t)$. Exactly at $R(0) = R_c$ the turbulence decays asymptotically at constant Reynolds number, denoted as R_c'. The main purpose of this section will be to show that this decay takes place with a constant and nonzero value for the parameter x, defined in (6).

The decay of the turbulence at constant Reynolds number R_c' allows exact analytical solution for the asymptotic evolution of the energy and enstrophy, related by

$$\frac{d}{dt}\langle \mathbf{u}^2 \rangle = -2\nu \langle \omega^2 \rangle. \tag{43}$$

Replacing $\langle \omega^2 \rangle$ in favor of $\langle \mathbf{u}^2 \rangle$ and R_c' by means of (42), one obtains the closed evolution equation

$$\frac{d}{dt}\langle \mathbf{u}^2 \rangle = -\frac{2}{\nu R_c'^2}\langle \mathbf{u}^2 \rangle^2, \tag{44}$$

which has analytical solution. The asymptotic solution of (44) at large times is given by[18]

$$\langle \mathbf{u}^2 \rangle = \tfrac{1}{2}\nu R_c'^2 t^{-1}, \quad \langle \omega^2 \rangle = \tfrac{1}{4} R_c'^2 t^{-2}, \tag{45}$$

where the solution for the enstrophy is determined from (43). The only unknown parameter in (45) is R_c' and its computation is easily obtained from relatively low resolution numerical simulations.

Although the precise value of the asymptotically constant Reynolds number R_c' depends on the particular choice of initial conditions for the flow field, there is another nondimensional group which takes a unique value. Taking the time derivative of the Reynolds number (42), and using (43) and the corresponding time-evolution equation for the enstrophy in two-dimensional turbulence, given by

$$\frac{d}{dt}\langle \omega^2 \rangle = -2\nu \langle (\boldsymbol{\nabla}\omega)^2 \rangle, \tag{46}$$

one determines the following evolution equation for $R(t)$:

$$\frac{d}{dt} R = (\rho^2 - 2)\langle \omega^2 \rangle^{1/2}, \tag{47}$$

where the nondimensional group ρ is defined by

$$\rho = \frac{\langle \mathbf{u}^2 \rangle^{1/2} \langle (\boldsymbol{\nabla}\omega)^2 \rangle^{1/2}}{\langle \omega^2 \rangle}. \tag{48}$$

From (47), two-dimensional turbulence decay at constant Reynolds number is observed to occur when $\rho = \sqrt{2}$.

The parameter x, defined in (6), is now easily determined. Using the identity $\epsilon/\nu = \langle \omega^2 \rangle$ and (45), one finds that x is nonzero during the decay with constant value

$$x = 1/R_c'. \tag{49}$$

It is also clear that y, defined in (6), will be constant for the transport of a passive scalar field provided ϵ_θ evolves as a power law in time.

Furthermore, at the critical Reynolds number the energy spectrum $E(k,t)$ decays self-similarly over all wave numbers. If we impose the normalization of the self-similar spectrum $\hat{E}(\hat{k})$ to be

$$\int_0^\infty \hat{E}(\hat{k})\, d\hat{k} = \int_0^\infty \hat{k}^2 \hat{E}(\hat{k})\, d\hat{k} = \frac{1}{2}, \tag{50}$$

then the scaling of the spectrum and wave number is given explicitly by

$$E(k,t) = \frac{\sqrt{2}}{2}\, \nu^{3/2} R_c'^2 t^{-1/2} \hat{E}(\hat{k}); \quad \hat{k} = (2\nu t)^{1/2} k. \tag{51}$$

We note here that the factors of R_c' in this scaling differ from that obtained using the Kolmogorov scaling of (2) and (3), though this is of little importance.

We now demonstrate these results by numerical simulation. The initial conditions of the flow field are the same as used previously,[18] with the initial energy spectrum specified in general by

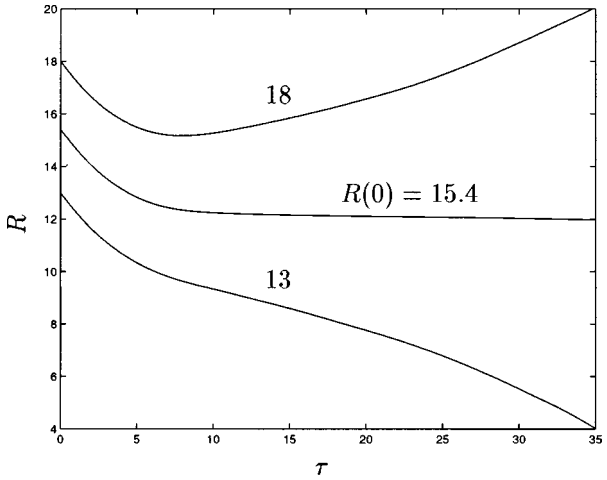

FIG. 4. Time evolution of the Reynolds number $R(t)$ for initial values $R(0) = 13$, 15.4 and 18.

$$E(k,0) = \frac{1}{2} a_n u_0^2 k_p^{-1} \left(\frac{k}{k_p}\right)^{2n+1} \exp\left[-\left(n+\frac{1}{2}\right)\left(\frac{k}{k_p}\right)^2\right], \tag{52}$$

with $a_n = (2n+1)^{n+1}/2^n n!$ and $n = 3$. The initial values of $\langle \mathbf{u}^2 \rangle$ and $\langle \omega^2 \rangle$ are determined from (52) to be

$$\langle \mathbf{u}^2 \rangle(0) = u_0^2, \quad \omega_0^2 \equiv \langle \omega^2 \rangle(0) = \frac{2n+2}{2n+1} u_0^2 k_p^2, \tag{53}$$

so that the initial Reynolds number (42) of the turbulence with $n = 3$ is given by

$$R(0) = \sqrt{\frac{7}{8}} \frac{u_0}{k_p \nu}. \tag{54}$$

In Fig. 4, the evolution of the Reynolds number $R(t)$ versus $\tau(t)$ is shown for initial values above and below the critical value R_c, and at $R_c = 15.4$, where

$$\tau = \int_0^t dt \langle \omega^2 \rangle^{1/2}. \tag{55}$$

The value for R_c obtained here is slightly less than that reported earlier[18] due to the better resolution of the initial conditions in the present simulations. In Fig. 5, the decay of the energy and enstrophy are compared to the analytical results (45), with $R_c' = 12.0$ obtained from Fig. 4. Excellent agreement between the simulation and the theoretical scaling laws is observed. As seen from Fig. 4, the analytical solution given by (45) is unstable to perturbations in $R(0) = R_c$, with values slightly lower or higher resulting in asymptotically decreasing or increasing Reynolds numbers, respectively. In other words, $\rho = \sqrt{2}$ is an unstable fixed point of (47).

In Fig. 6, the time evolution of the energy spectrum $E(k,t)/u_0^2 l_0$ versus wave number $k l_0$, with $l_0 = u_0/\omega_0$, at the times $\tau = 0,5,10,\ldots,30$ is plotted. The spectra are smoother than those computed earlier[18] as a consequence of ensemble-averaging over a large number (64) of independent realizations. In Fig. 7, the self-similar spectrum $\hat{E}(\hat{k})$ versus

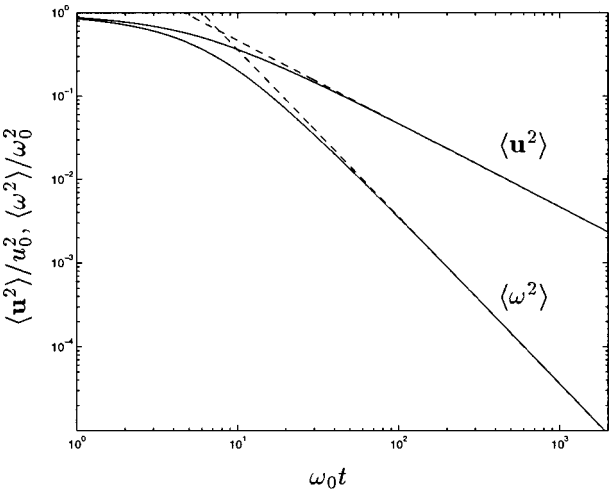

FIG. 5. Time evolution of the energy and enstrophy for $R(0)=15.4$ compared to the analytical results (dashed lines).

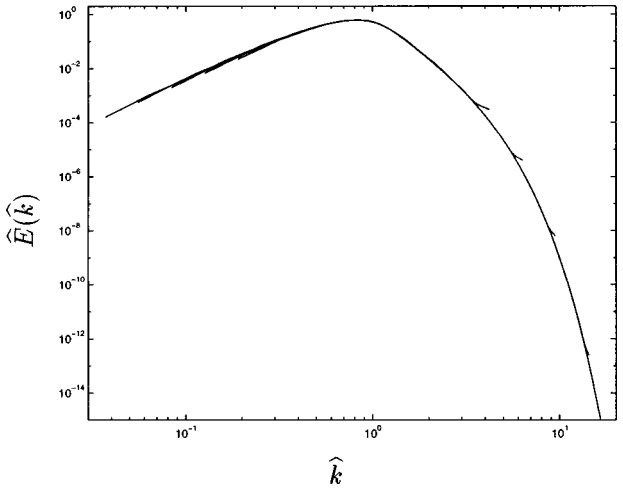

FIG. 7. Rescaling of the energy spectrum of Fig. 6. The times plotted correspond to $\tau=10,15,\ldots,30$.

$\hat{k}$ is plotted at the times $\tau=10,15,\ldots,30$. A near-perfect collapse of the spectra is found indicating that the scaling given by (51) is exact.

VI. PASSIVE SCALAR TRANSPORT WITH UNIFORM MEAN GRADIENT

A. Theoretical considerations

We now consider the transport of a passive scalar field with nonzero uniform mean gradient. The transport equation for the fluctuating scalar field is given by (7), where the source of scalar variance is

$$f_\theta=\beta u_1. \tag{56}$$

In (56), β is the negative of the gradient of the mean scalar field in the x_1 direction, assumed here to be constant in space and time. The scalar fluctuations are taken to be zero at the initial instant and are subsequently generated by velocity fluctuations along the mean gradient.

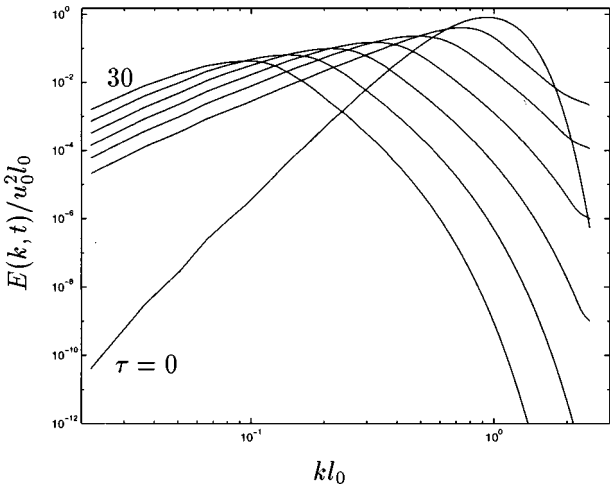

FIG. 6. Evolution of the energy spectrum in time with $R(0)=15.4$. The times plotted correspond to $\tau=0,5,10,\ldots,30$.

We thus consider in this section only the situation for which $\beta\neq 0$, its precise value being unimportant. In the next section we consider further the freely-decaying scalar problem with $\beta=0$.

The scalar equation (7) introduces a single additional nondimensional group to the problem: the Schmidt number σ. Our study of the viscous-convective subrange is concerned with the asymptotic statistical laws of the scalar decay at large σ.

An equation for the scalar variance may be determined from (7) using (56) to be

$$\frac{d\langle\theta^2\rangle}{dt}=2\beta\langle u_1\theta\rangle-2\epsilon_\theta, \tag{57}$$

where the scalar-variance dissipation rate is defined as

$$\epsilon_\theta=D\langle(\nabla\theta)^2\rangle. \tag{58}$$

We will later see that a closure of (57) is possible for turbulence decay at constant Reynolds number as $D\to 0$, but at this point we ascertain the asymptotic evolution of the scalar variance by dimensional arguments alone.

From the scalar equation (7) combined with (56), it is evident that the scalar field itself is proportional to β. If we further assume that, asymptotically, the only other dimensional quantities of relevance are the viscosity ν (or diffusivity D) and the time t, then the only dimensionally correct form for the scalar variance is

$$\langle\theta^2\rangle\propto\beta^2\nu t, \tag{59}$$

where the coefficient of proportionality can depend only on the two nondimensional groups of our problem, namely R_c' which is a fixed constant, and σ.

It is reasonable to suppose that the three separate terms in the budget equation for the scalar variance, (57), have the same time dependence so that from (59), the scalar-variance cascade rate ϵ_θ must become constant, asymptotically. Thus we have determined that the parameter y, defined in (14), is identically zero for this flow.

TABLE I. For $\beta \neq 0$, resolution N^2 and realizations M for scalar with Schmidt number σ. The wave number k_p is that for which the initial energy spectrum is maximum.

σ	$N^2 \times M$	k_p
1	$512^2 \times 64$	64
10	$512^2 \times 64$	64
10^2	$1024^2 \times 16$	64
10^3	$1024^2 \times 16$	16
10^4	$4096^2 \times 2$	16

In summary, for decaying two-dimensional turbulence at constant Reynolds number transporting a passive scalar field with nonzero uniform mean gradient, the parameters x and y introduced in Secs. I and II are constants, independent of time. The results of Sec. III are thus applicable. In particular, with x given by (49) and $y=0$, the Kraichnan transfer spectrum predicts a $k^{-(1+s)}$ viscous-convective subrange spectrum, with s given by [see (34)]

$$s = \frac{1+\alpha R_c'}{\alpha R_c'}\left[\left(1+\frac{4\alpha R_c'}{(1+\alpha R_c')^2}\right)^{1/2}-1\right] \approx 0.56, \tag{60}$$

where we have used $R_c' = 12.0$ and $\alpha^{-1} = 6.0$. The viscous-convective subrange thus predicted for this flow has approximate power-law form $k^{-1.56}$, significantly different than the stationary solution k^{-1}.

B. Numerical simulations

We now present numerical results for the scalar statistics. The number of grid points N in the two directions and the number of independent realizations M over which an ensemble average is taken is shown in Table I for the simulated Schmidt numbers. Also shown is the value of k_p chosen for which the initial energy spectrum (52) is maximum. For large σ, better small-scale resolution is necessary so that either the number of grid points N must be increased or the value of k_p decreased. The simulations for $\sigma = 1$ and 10 were performed with 64 independent realizations running simultaneously on 64 processors of a parallel machine, with the statistical averaging performed across processors. This allowed for the writing of a very efficient numerical code. The higher resolution calculations were performed with single realizations spread out on multiple processors, and with all the realizations done in parallel.

The logarithmic derivative in time (power-law exponent) of the scalar variance versus the normalized time τ, (55), for all of the different Schmidt numbers is plotted in Fig. 8. The logarithmic derivative is two at the smallest times indicating a t^2 initial growth of scalar fluctuations due to a constant fluid motion along the mean scalar gradient (see (7) and (56)). Asymptotically, the power-law exponent becomes one (indicated by a dashed line) for all Schmidt numbers, as predicted in (59). The large fluctuations in the curve for $\sigma = 10^4$ are due to the poor statistical average. This calculation was too expensive to make additional averaging worthwhile.

For $\sigma = 100$, the time evolution of the scalar-variance spectrum $E_\theta/(\beta^2 l_0^3)$ is shown in Fig. 9. At the earliest times of evolution, the scalar field is slightly under-resolved, but

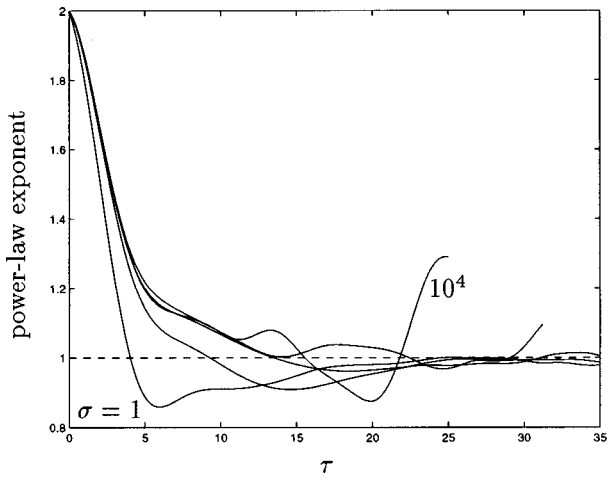

FIG. 8. Time evolution of the power-law exponent of the scalar-variance for nonzero β. The solid lines are the results of the simulations for Schmidt numbers $1,10,\ldots,10^4$ and the dashed line is the theoretical result.

becomes sufficiently well-resolved at the latest times. The times plotted correspond to $\tau = 5,10,\ldots,35$, with τ defined in (55). The largest scales of the flow are still well captured by the computational box at the last time computed.

The scalar-variance spectra at the times $\tau = 20,25,\ldots,35$ are normalized using Batchelor scaling (11) and plotted versus the normalized wave number $\hat{k} = k/k_B$ in Fig. 10. The spectra are observed to collapse over all wave numbers, indicating that the scalar-variance spectrum evolves in a completely self-similar fashion together with the energy spectrum. This self-similar evolution in time was observed for all simulated Schmidt numbers.

Of primary interest to us here is the plot of the different Schmidt number scalar-variance spectra normalized by Batchelor scaling. This is shown in Fig. 11, where the results for $\sigma = 1,10,10^2,10^3,10^4$ are plotted at the times corresponding to $\tau = 35,35,35,30,20$, respectively. A reasonable collapse of all the spectra, excepting the lowest wave numbers not contained in the viscous subrange, is observed. Also

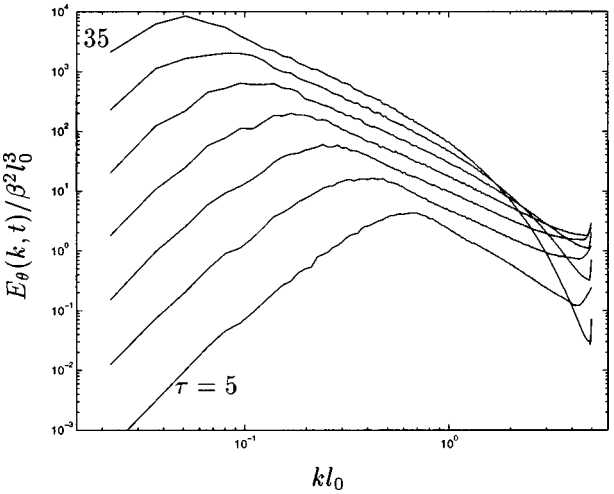

FIG. 9. Evolution of the scalar-variance spectrum in time with $\sigma = 100$. The times plotted correspond to $\tau = 5,10,\ldots,35$.

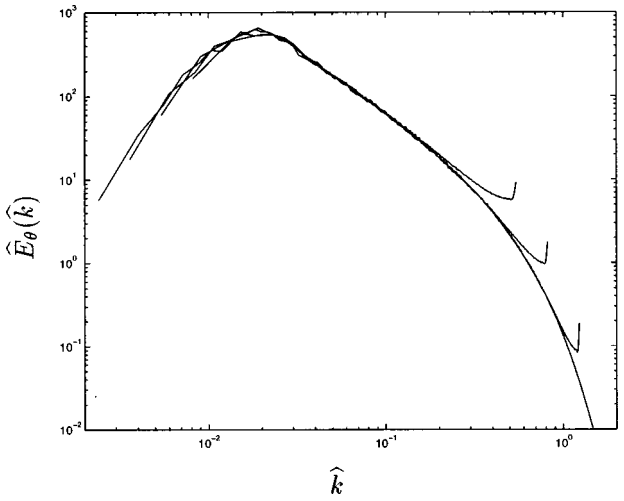

FIG. 10. Rescaling of the scalar-variance spectrum of Fig. 9. The times plotted correspond to $\tau=20,25,\ldots,35$.

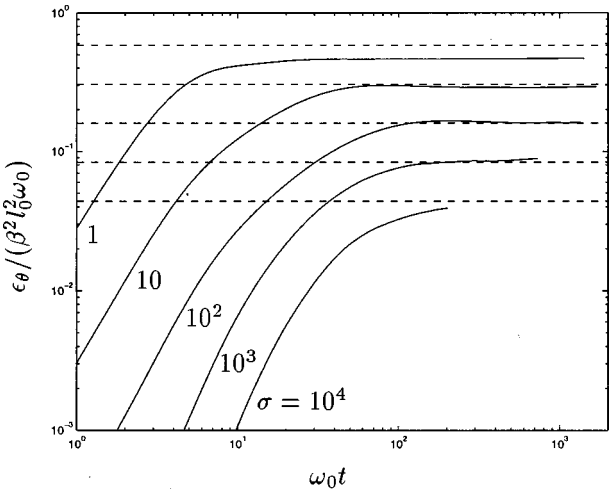

FIG. 12. Time evolution of the scalar-variance dissipation rate ϵ_θ for all σ. The asymptotic theoretical predictions are plotted as dashed lines, obtained using as a reference value the numerical result for $\sigma=100$.

shown in Fig. 11 by the dashed line is the spectrum obtained using the Kraichnan form of the transfer, (24), with $\alpha^{-1}=6.0$, $x=1/R_c'$, and $y=0$. Good (but not perfect) agreement between the simulation and theoretical results is observed, including the prediction of a viscous-convective subrange of approximate power-law form $k^{-1.56}$.

A secondary prediction of the theoretical analysis is the dependence of the scalar-variance dissipation rate ϵ_θ on the anomalous power-law exponent of the viscous-convective subrange. (For a discussion with respect to the Batchelor form for the transfer, see the paragraph preceeding (23).) The prediction using Kraichnan's form for the transfer is

$$\epsilon_\theta=\sigma^{-s/2}\chi, \tag{61}$$

where χ is independent of σ, and s is given by (60). In Fig. 12, the scalar-variance dissipation rate $\epsilon_\theta/(\beta^2 l_0^2\omega_0)$ versus time $\omega_0 t$ is plotted for all the Schmidt numbers. Also shown by the dashed lines are the predictions of (61) with $s=0.56$, obtained by using as a reference value the numerical simulation asymptotic result $\epsilon_\theta/(\beta^2 l_0^2\omega_0)=0.16$ when $\sigma=100$. Excepting $\sigma=1$, it is observed that (61) agrees reasonably well with the data. The $\sigma=10^4$ computation was not evolved sufficiently long to attain clear asymptotics, but the trend is in agreement with the theoretical prediction.

It is evident from Fig. 12 that the scalar dissipation approaches zero as $\sigma\to\infty$. The scalar-variance evolution equation (57) becomes in this limit

$$\frac{d\langle\theta^2\rangle}{dt}=2\beta\langle u_1\theta\rangle. \tag{62}$$

It thus becomes possible to close (62) with a simple hypothesis on the scalar-velocity correlation; namely,

$$\langle u_1\theta\rangle=\alpha\langle u_1^2\rangle^{1/2}\langle\theta^2\rangle^{1/2}, \tag{63}$$

with α constant as $\sigma\to\infty$. Since the two-dimensional turbulence is statistically isotropic in space, we also have

$$\langle u_1^2\rangle=\tfrac{1}{2}\langle\mathbf{u}^2\rangle, \tag{64}$$

with $\langle\mathbf{u}^2\rangle$ given asymptotically by (45). The correlation coefficient α may be found numerically, and Fig. 13 provides a plot for the different σ simulations. An asymptotic value of $\alpha\approx 0.45$ as $\sigma\to\infty$ seems reasonable, though the statistics of the computations become noticeably poorer for $\sigma=10^3$ and 10^4.

Thus combining (62)–(64), one obtains the differential equation

$$\frac{d\langle\theta^2\rangle}{dt}=\sqrt{2}\alpha\beta\langle\mathbf{u}^2\rangle^{1/2}\langle\theta^2\rangle^{1/2}, \tag{65}$$

which may be solved analytically using (45). The asymptotic solution is

$$\langle\theta^2\rangle=\alpha^2\beta^2\nu R_c'^{\,2}t, \tag{66}$$

in agreement with the prediction of (59), determined using dimensional analysis. Here, we exhibit the proportionality constants explicitly.

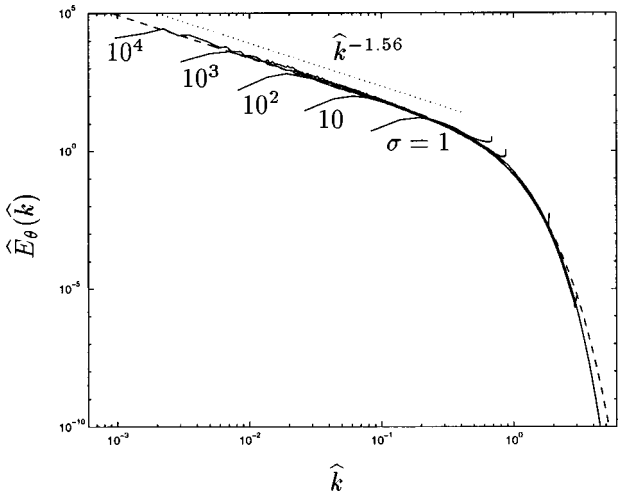

FIG. 11. Batchelor-scaled scalar-variance spectra for all σ. The dashed line is the theoretical result obtained using the Kraichnan form for the transfer. For comparison, the power law $\hat{k}^{-1.56}$ is shown by the dotted line.

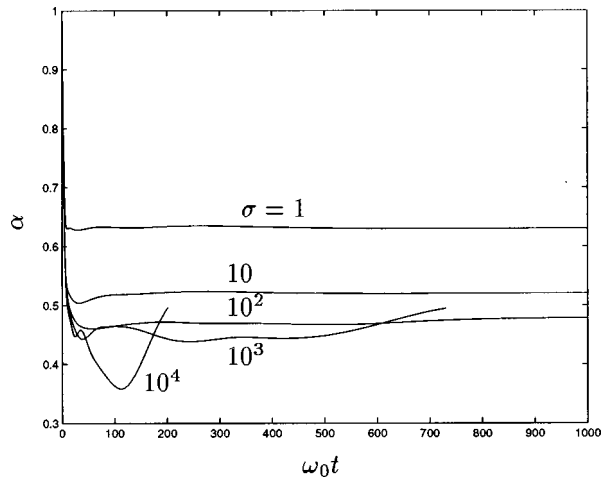

FIG. 13. Time evolution of the scalar-velocity correlation coefficient α for all σ.

VII. PASSIVE SCALAR TRANSPORT WITHOUT MEAN GRADIENT

A. Theoretical considerations

Decaying scalar fluctuations with $\beta=0$ in two-dimensional turbulence was considered by Lesieur and Herring,[20] and the decay laws were shown to depend on the form of the initial scalar-variance spectrum at low wave numbers. Here, we assume that an asymptotic expansion of the scalar-variance spectrum can be written as

$$E_\theta(k,t)=\pi k(C_0+k^2C_2+\dots) \tag{67}$$

as $k\to 0$. It is known that the low wave number coefficient C_0 is an invariant,[21] and if zero initially, then C_2 is necessarily nonzero and time dependent due to nonlinear transfer of scalar variance from small-to-large scales.[22]

Asymptotic decay laws of the scalar variance can be determined from a dimensional analysis[23] by postulating a linear dependence (due to the linearity of the scalar transport equation) on the leading-order coefficient of (67), and a dependence on ν (or D) and t, only. For $C_0\neq 0$, the decay law is determined to be

$$\langle\theta^2\rangle\propto C_0(\nu t)^{-1}, \tag{68}$$

where the proportionality constant can depend on R_c', which is fixed, and σ.

For $C_0=0$, the asymptotic time behavior of C_2 is unknown and we postulate it to be of power-law form

$$C_2(t)=ct^\gamma, \tag{69}$$

where $\gamma>0$ is an unknown exponent and c is a dimensional constant which could depend on initial conditions. The decay law of the scalar variance is thus determined by dimensional analysis to be

$$\langle\theta^2\rangle\propto C_2(\nu t)^{-2}=c\nu^{-2}t^{-2+\gamma}. \tag{70}$$

The evolution equation for the scalar variance is given by (57) with $\beta=0$, and using (45), (68), and (70) one can determine the parameter y, defined in (14):

TABLE II. For $C_0\neq 0$, resolution N^2 and realizations M for scalar with Schmidt number σ. The wave number k_p is that for which the initial spectra are maximum.

σ	$N^2\times M$	k_p
1	$1024^2\times 32$	128
10	$2048^2\times 8$	128
10^2	$2048^2\times 8$	64

$$y=-\frac{4}{R_c'},\quad C_0\neq 0;\quad y=-\frac{(6-2\gamma)}{R_c'},\quad C_0=0. \tag{71}$$

Together with $x=1/R_c'$, $\alpha^{-1}=6.0$, $R_c'=12.0$, the anomolous exponent s in the viscous-convective subrange spectrum $k^{-(1+s)}$, derived in (34) from the Kraichnan model, is found to be

$$s=\frac{1+\alpha R_c'}{\alpha R_c'}\left[\left(1-\frac{4\alpha R_c'}{(1+\alpha R_c')^2}\right)^{1/2}-1\right]\approx -1.0,$$
$$C_0\neq 0; \tag{72}$$

$$s=\frac{1+\alpha R_c'}{\alpha R_c'}\left[\left(1-\frac{4\alpha R_c'(2-\gamma)}{(1+\alpha R_c')^2}\right)^{1/2}-1\right]$$
$$\approx \tfrac{1}{2}[(-7.0+8.0\gamma)^{1/2}-3.0],\quad C_0=0. \tag{73}$$

For $C_0\neq 0$, the viscous-convective subrange spectrum is approximately independent of wave number, i.e., the spectrum is proportional to $k^{0.0}$. For $C_0=0$, if $\gamma<7/8$ then s is complex. Recalling (32) and (33), a complex s implies a solution for $f(r)$ which is oscillatory as $r\to 0$, taking on negative values. This would result in the unrealizable situation of a negative scalar-variance spectrum, implying a breakdown of our theoretical analysis. On the other hand, a value $\gamma\geqslant 7/8$ results in s being real, and also implies from (70) a decay law of the scalar variance less steep than $t^{-9/8}$. We know of no way to accurately estimate γ other than by numerical simulations.

B. Numerical simulations: $C_0\neq 0$

The form of our initial scalar-variance spectrum is taken to be the same as for the energy spectrum, (52), replacing u_0 by θ_0. Here, we consider $n=0$ corresponding to a low wave number scalar-variance spectrum proportional to $\pi C_0 k$, with the invariant C_0 given by

$$C_0=\frac{\theta_0^2}{2\pi k_p^2}. \tag{74}$$

The case of $C_0=0$ initially will be treated in Part C. Table II shows the resolution, number of realizations, and value of k_p used in the present calculations. A numerical simulation of a decaying scalar field without mean gradient requires more resolution for a given value of σ than those performed with nonzero mean gradient, primarily because of the more rapid loss of statistical sample of the largest scales. We have thus only been able to obtain reasonably accurate results to a maximum Schmidt number of $\sigma=100$.

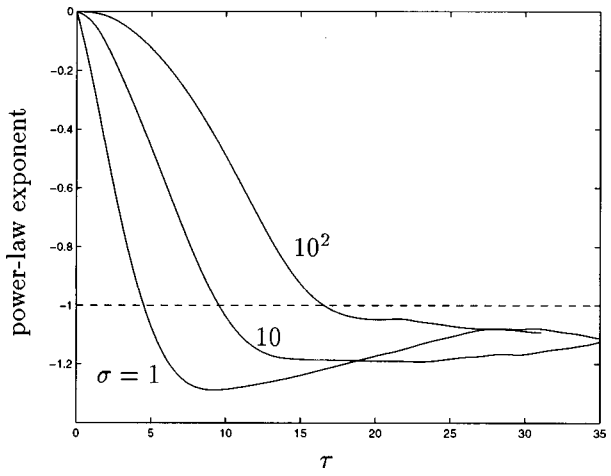

FIG. 14. Time evolution of the power-law exponent of the scalar-variance for $C_0 \neq 0$. The solid lines are the results of the simulations for Schmidt numbers 1, 10, 10^2 and the dashed line is the theoretical result.

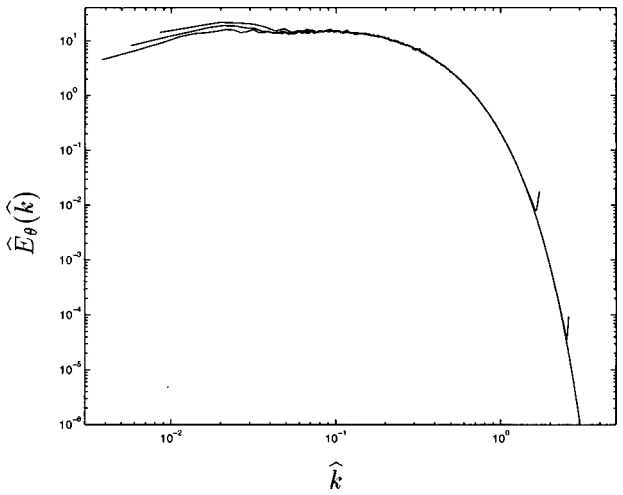

FIG. 16. Batchelor scaling of the scalar-variance spectrum of Fig. 15. The times plotted correspond to $\tau = 20,25,30$.

In Fig. 14, the logarithmic derivative in time of the scalar variance versus τ is plotted with the dashed line showing the expected asymptotic power-law exponent obtained from (68). At large times, the power-law exponent obtained from the simulation data deviates about 10% from the predicted exponent. This is to be compared to calculations done with a mean scalar gradient, Fig. 8, for which agreement between the simulations and theoretical scalings was noticeably better.

In Fig. 15, the time evolution of the scalar-variance spectrum for Schmidt number $\sigma = 10$ is shown, corresponding to the times $\tau = 0,5,10,\ldots,30$. It is evident that the low wave number coefficient is an invariant, but that there is little large scale sample remaining at the last time plotted. In Fig. 16, the times corresponding to $\tau = 20,25,30$ are rescaled according to Batchelor scaling, (11). The spectrum appears to decay self-similarly, with some deviation from self-similarity occurring at the smallest wave numbers. We suspect that this is due to the adverse influence of the periodic boundary conditions on the largest scales of the flow. This error may also account for the discrepancy between the theoretical decay exponent and that obtained from the simulations.

All three Schmidt number spectra at times corresponding to $\tau = 30$ are rescaled according to Batchelor scaling and plotted in Fig. 17. A reasonable collapse of the three spectra is observed. Also shown by the dashed line is the spectrum obtained using the Kraichnan form of the transfer with $\alpha^{-1} = 6.0$, $x = 1/R_c'$, $y = -4/R_c'$, $R_c' = 12.0$. Reasonable (but not perfect) agreement between the simulations and the theoretical result is observed, including the prediction of a viscous-convective subrange which is approximately independent of wave number.

A secondary prediction of the theoretical analysis is that the scalar-variance dissipation scales like $\epsilon_\theta = \sigma^{1/2}\chi$ (from (61) and (72)). In Fig. 18, the dissipation rate is plotted versus time together with the theoretical predictions, obtained by using as a reference value the asymptotic decay of the scalar variance when $\sigma = 100$. The agreement between the

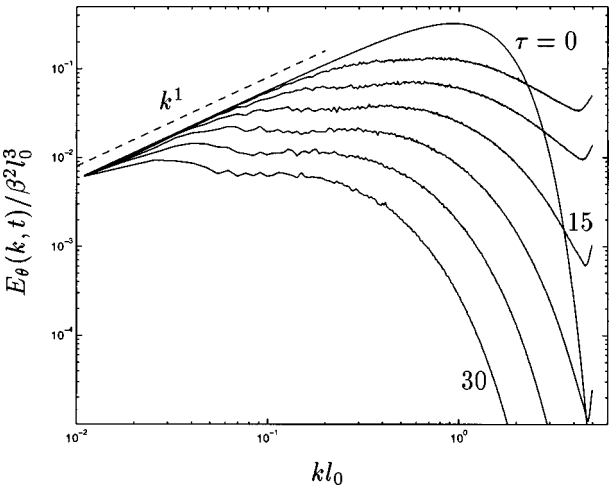

FIG. 15. Evolution of the scalar-variance spectrum in time with $C_0 \neq 0$ and $\sigma = 10$. The times plotted correspond to $\tau = 0,5,10,\ldots,30$.

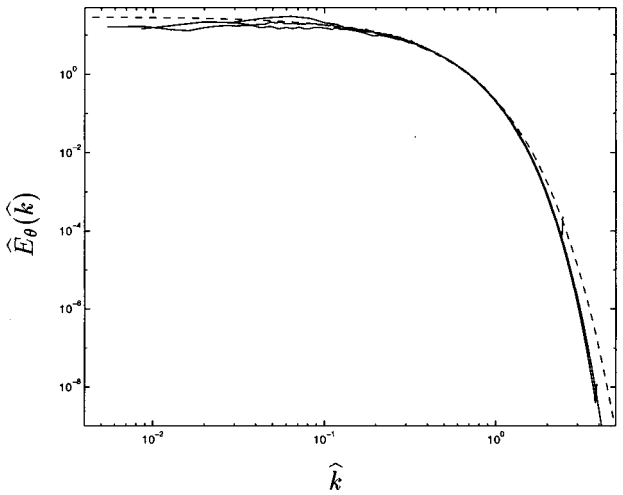

FIG. 17. Batchelor-scaled scalar-variance spectra for all σ. The dashed line is the theoretical result obtained using the Kraichnan form for the transfer. The asymptotic form of the theoretical spectrum is $\hat{k}^{0.0}$ as $\hat{k} \to 0$.

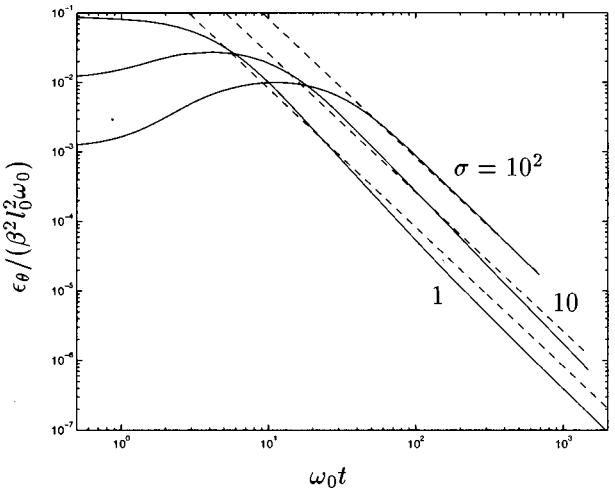

FIG. 18. Time evolution of the scalar-variance dissipation rate ϵ_θ for $\sigma = 1,10,100$. The asymptotic theoretical predictions are plotted as dashed lines, obtained using as a reference value the numerical result for $\sigma = 100$.

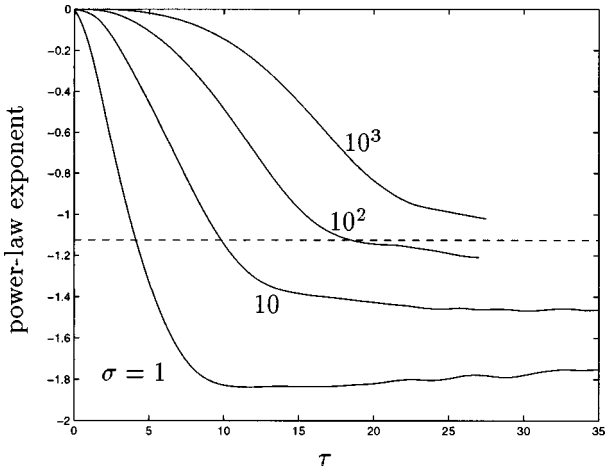

FIG. 19. Time evolution of the power-law exponent of the scalar variance for $C_0 = 0$. The solid lines are the results of the simulations for Schmidt numbers $1,10,10^2,10^3$ and the dashed line separates theoretically predicted real from complex values of s.

predicted and observed behavior is reasonable for $\sigma = 10$ but has substantial error for $\sigma = 1$, for which the Schmidt number is most likely too small.

C. Numerical simulations: $C_0 = 0$

We now consider an initial scalar-variance spectrum with form (52) and $n = 3$. The low wave number coefficients C_0 and C_2 in (67) are initially zero; C_0 remains zero and C_2 increases in time. Table III shows the resolution, number of realizations, and value of k_p used in the present calculations.

In Fig. 19, the logarithmic derivative in time of the scalar variance versus τ is plotted. There does not appear to be a universal asymptotic decay exponent for this flow, and the magnitude of the decay exponent decreases with increasing Schmidt number. If (69) and (70) are to be believed, this implies that the exponent γ increases with Schmidt number. From a rough estimate of the asymptotic power-law exponents of the scalar-variance decay, a value of γ can be determined for the different Schmidt numbers. The estimated decay exponents and inferred values of γ are shown in Table IV.

Also shown in Fig. 19 for future reference is a dashed line which indicates the value of the decay law for which the theoretical exponent s in (73) changes from real to complex; (below the dashed line s is complex and above it is real).

In Fig. 20, the time evolution of the scalar-variance spectrum for Schmidt number $\sigma = 10$ is shown, corresponding to the times $\tau = 0,5,10,\ldots,30$. The formation of a low wave number scalar-variance spectrum proportional to k^3 is evident. In Fig. 21, the times corresponding to $\tau = 20,25,30$ are rescaled according to Batchelor scaling, (11). The spectrum is observed to decay self-similarly over all wave numbers.

All four Schmidt number spectra at time $\tau = 25$ are rescaled according to Batchelor scaling and plotted in Fig. 22. The spectra are observed to collapse in the diffusion subrange, but not in the convective subrange or at the largest scales. Also shown by the dashed lines are the spectra obtained from the Kraichnan model with $\alpha^{-1} = 6.0$, $x = 1/R_c'$, $y = -(6-2\gamma)/R_c'$, $R_c' = 12.0$, and inferred values of γ shown in Table IV. All of the theoretical results collapse in the diffusive subrange at large $\hat{k}$ but differ at small wave numbers. This collapse of the theoretical spectra at large $\hat{k}$ can be shown from the results of Sec. III, where the asymptotic form of the spectrum given by (35) is seen to be independent of y, and therefore γ. The form of the spectrum in the convective subrange, however, does depend on γ.

There is little direct numerical evidence from Fig. 22 for a power-law form of the spectrum in the viscous-convective subrange. Nevertheless, it is interesting to observe that the Kraichnan model for the transfer agrees reasonably well with the simulation data for relatively small values of σ despite predicting a complex value for the anomalous exponent s (see Fig. 19). Apparently, for σ less than about 100, a viscous-convective subrange has not yet developed so that the range of wave numbers over which the theoretical spec-

TABLE III. For $C_0 = 0$, resolution N^2 and realizations M for scalar with Schmidt number σ. The wave number k_p is that for which the initial spectra are maximum.

σ	$N^2 \times M$	k_p
1	$1024^2 \times 16$	128
10	$2048^2 \times 8$	128
10^2	$2048^2 \times 8$	64
10^3	$4094^2 \times 2$	64

TABLE IV. For $C_0 = 0$, estimated exponents of the scalar-variance and the inferred values of the exponent γ.

σ	Decay exponent	γ
1	-1.8	0.2
10	-1.45	0.55
10^2	-1.2	0.8
10^3	-1.0	1.0

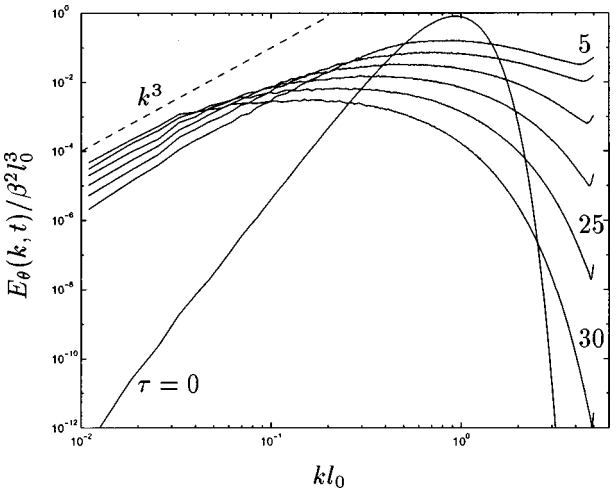

FIG. 20. Evolution of the scalar-variance spectrum in time with $C_0 \neq 0$ and $\sigma = 10$. The times plotted correspond to $\tau = 0,5,10,\ldots,30$.

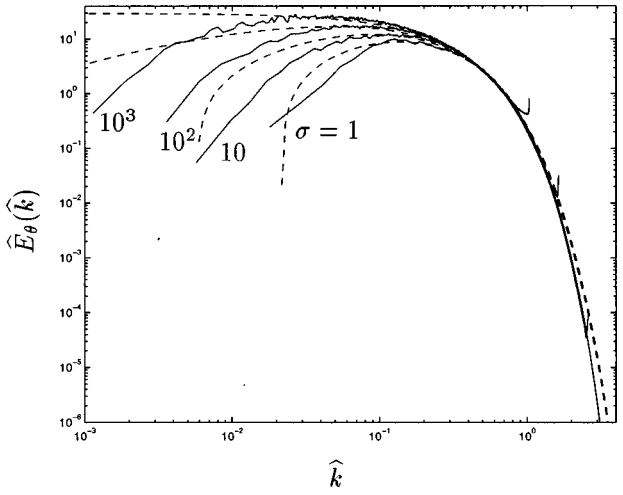

FIG. 22. Batchelor-scaled scalar-variance spectra for all σ. The dashed lines are the theoretical results obtained using the Kraichnan form for the transfer.

trum is oscillatory is not part of the universal subrange. For σ greater than about 100, γ is large enough so that the exponent s is real; apparently for these larger values of σ a viscous-convective subrange of power-law form will begin to develop. It is reasonable to expect that as $\sigma \to \infty$, the power-law exponent of the scalar-variance decay will approach some limiting value as will the exponent γ. It seems a value of σ much large than 1000 is required to observe approximate asymptotic behavior.

VIII. CONCLUSIONS

We have derived necessary conditions so that a nonstationary high Schmidt number passive scalar field may follow Batchelor scaling in the viscous-convective subrange. In three dimensions, these conditions can be approximately satisfied for large Reynolds numbers. However, Batchelor scaling is also possible if the enstrophy of the turbulence decays as t^{-2}. Just such a decay was recently discovered in a study of two-dimensional turbulence decaying at constant Reynolds number,[18] and we have investigated in detail the transport of passive scalars by this type of decaying turbulence.

Being unstable to small perturbations, decaying two-dimensional turbulence at constant Reynolds number is unlikely to be observed in nature. Nevertheless, this flow provides us an interesting numerical test of Batchelor scaling in high Schmidt number fluids, and in particular a test of the accuracy of the model scalar-variance transfer spectrum proposed by Kraichnan.[4] There are some laboratory[9,10] and numerical experiments[14] in which Batchelor's k^{-1} spectrum is not observed and this has led to suggestions that Batchelor's result may not be universal[9] or may be fundamentally flawed.[14] The present work at least provides additional numerical support in favor of Batchelor scaling, and further demonstrates the accuracy of Kraichnan's model for stationary and nonstationary flow situations.

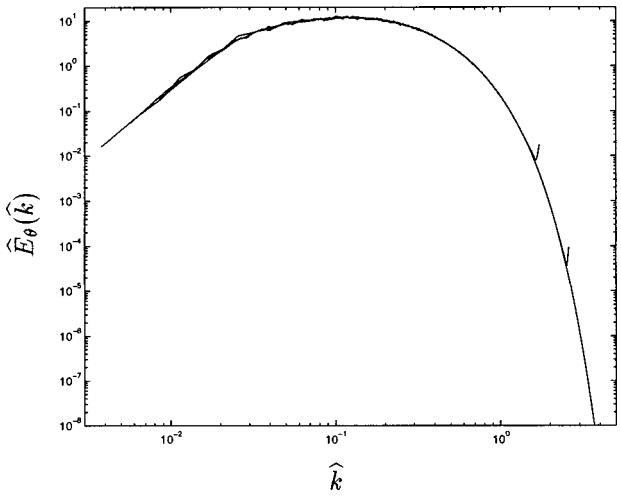

FIG. 21. Batchelor scaling of the scalar-variance spectrum of Fig. 20. The times plotted correspond to $\tau = 20,25,30$.

ACKNOWLEDGMENTS

I wish to thank A. Wray and R. Rogallo for allowing me use of their simulation software. The support of the Hong Kong Research Grant Council is gratefully acknowledged. The computations presented here were performed on an Intel Paragon at The Hong Kong University of Science & Technology.

[1] G. K. Batchelor, ''Small-scale variation of convected quantities like temperature in a turbulent field. Part 1. General discussion and the case of small conductivity,'' J. Fluid Mech. **5**, 113 (1959).
[2] P. G. Saffman, ''On the fine-scale structure of vector fields convected by a turbulent fluid,'' J. Fluid Mech. **16**, 545 (1963).
[3] R. H. Kraichnan, ''Small-scale structure of a scalar field convected by turbulence,'' Phys. Fluids **11**, 945 (1968).
[4] R. H. Kraichnan, ''Convection of a passive scalar by a quasi-uniform random straining field,'' J. Fluid Mech. **64**, 737 (1974).
[5] C. H. Gibson and W. H. Schwarz, ''The universal equilibrium spectra of turbulent velocity and scalar fields,'' J. Fluid Mech. **16**, 365 (1963).
[6] H. L. Grant, B. A. Hughes, W. M. Vogel, and A. Moilliet, ''The spectrum of temperature fluctuations in turbulent flow,'' J. Fluid Mech. **34**, 423 (1968).
[7] J. O. Nye and R. S. Brodkey, ''The scalar spectrum in the viscous-convective subrange,'' J. Fluid Mech. **29**, 151 (1967).

[8]X. I. Wu, B. Martin, H. Kellay, and W. I. Goldburg, ''Hydrodynamic convection in a two-dimensional Couette cell,'' Phys. Rev. Lett. **75**, 236 (1995).
[9]P. L. Miller and P. E. Dimotakis, ''Measurements of scalar power spectra in high Schmidt number turbulent jets,'' J. Fluid Mech. **308**, 129 (1996).
[10]B. S. Williams, D. Marteau, and J. P. Gollub, ''Mixing of a passive scalar in magnetically forced two-dimensional turbulence,'' Phys. Fluids **9**, 2061 (1997).
[11]M. Holzer and E. D. Siggia, ''Turbulent mixing of a passive scalar,'' Phys. Fluids **6**, 1820 (1994).
[12]T. M. Antonsen, F. F. Fan, and E. Ott, ''k spectrum of passive scalars in Lagrangian chaotic fluid flows,'' Phys. Rev. Lett. **75**, 1751 (1995).
[13]D. Bogucki, J. A. Domaradzki, and P. K. Yeung, ''Direct numerical simulations of passive scalars with $Pr>1$ advected by turbulent flow,'' J. Fluid Mech. **343**, 111 (1997).
[14]R. T. Pierrehumbert, ''Tracer microstructure in the large-eddy dominated regime,'' Chaos Solitons Fractals **4**, 1091 (1994).
[15]G. K. Batchelor, *The Theory of Homogeneous Turbulence* (Cambridge University Press, Cambridge, 1953).
[16]C. H. Gibson, ''Fine structure of scalar fields mixed by turbulence. II. Spectral theory,'' Phys. Fluids **11**, 2316 (1968).
[17]R. C. Mjolsness, ''Diffusion of a passive scalar at large Prandtl number according to the abridged Lagrangian interaction theory,'' Phys. Fluids **18**, 1393 (1975).
[18]J. R. Chasnov, ''On the decay of two-dimensional homogeneous turbulence,'' Phys. Fluids **9**, 171 (1997).
[19]L. M. Smith and V. Yakhot, ''Finite-size effects in forced two-dimensional turbulence,'' J. Fluid Mech. **274**, 115 (1994).
[20]M. Lesieur and J. Herring, ''Diffusion of a passive scalar in two-dimensional turbulence,'' J. Fluid Mech. **161**, 77 (1985).
[21]S. Corrsin, ''The decay of isotropic temperature fluctuations in an isotropic turbulence,'' J. Aeoronaut. Sci. **18**, 417 (1951).
[22]M. Lesieur, *Turbulence in Fluids* (Kluwer, Dordrecht, 1990).
[23]J. R. Chasnov, ''Similarity states of passive scalar transport in isotropic turbulence,'' Phys. Fluids **6**, 1036 (1994).